Materials Letters 366 (2024) 136501

Contents lists available at ScienceDirect

Materials Letters

journal homepage: www.elsevier.com/locate/matlet

Unraveling the connection of electronic and phononic structure with mechanical properties of commercial AZ80 alloy

Prince Sharma [a,b,*], Duane D. Johnson [a,c], Ganesh Balasubramanian [b], Prashant Singh [a,*]

[a] Ames Laboratory, U.S. Department of Energy, Iowa State University, Ames, IA 50011 USA
[b] Institute for Functional Materials and Devices, Lehigh University, Bethlehem, PA 18015, USA
[c] Department of Materials Science & Engineering, Iowa State University, Ames, IA 50011, USA

A B S T R A C T

Magnesium alloys, particularly in the aluminum-zinc (AZ) series, are widely recognized for their remarkable strength-to-weight ratio. We performed electronic structure, lattice dynamics, and mechanical properties of the AZ80 alloy using first-principles density-functional theory. The influence of dilute alloying by Al/Zn was observed in electronic-structure of AZ80 through hybridization of Mg-(*s,p*) with Al-*p*/Zn-*d* states. The Allen's electronegativity difference between Mg and Al/Zn was found to induce charge transfer mechanism that provides solid-solution strengthening and ductility, in agreement with experiments. The electronic and phononic band-structure was unfolded onto the primitive unit cell of pure Mg to provide key information related to structural distortions and disorder effects. Finally, the dynamic and mechanical stability of AZ80 were confirmed by phonons and Born-Huang criteria, respectively. Collectively, this study provides valuable insights into the fundamental properties of lightweight commercial grade AZ80, essential for application-oriented design of Mg alloys.

1. Introduction

Magnesium (Mg) and its alloys continue to gain attention for their promising applications in biomedical, automotive, and aerospace industries, owing to their exceptional strength-to-weight ratio and low density [1–3]. Incorporating Al and Zn in these alloys enhances corrosion resistance by promoting the formation of passivating oxide layers [4]. Additionally, improvements in castability, machinability, and heat treatment further enable us to optimize the properties of these alloys for potential manufacturability.

The AZ series, while maintaining Mg's light-weighting advantage, achieves a balance between strength and weight, crucial for industries, where both factors impact performance, durability, and efficiency in stressful environments [5,6]. Amongst them, the AZ80 alloy, with its Mg (91 %)-Al(7.8–9.2 %)-Zn(0.20–0.8 %) composition (a hexagonal-close-packed (*hcp*) lattice structure), stands out for its superior mechanical performance. Despite the wide popularity of the AZ series and other Mg-based alloys in the experimental literature, there exists limited understanding of their electronic and vibrational spectra, necessitating an in-depth examination of its electronic structure, lattice dynamics, and elastic properties. In this work, we employ first-principles density-functional theory (DFT) to calculate the underlying lattice dynamics and electronic structure of AZ80. We also scrutinize the interactions between lightweight Mg, Al, and heavy Zn atoms and their contribution to mass disorder that directly impacts thermal and mechanical properties [7,8].

2. Methods

We employ DFT as implemented in the pseudopotential-based *Vienna Ab-initio Simulation Package* [9,10] to achieve geometrical optimization and charge self-consistency. The generalized-gradient approximation (GGA) of Perdew, Burke and Ernzerhof (PBE) is employed [11] with a plane-wave cut-off energy of 520 eV. The choice of PBE over LDA or meta-GGA [12,13] functionals is based on the work of Söderling et al. [14] and Giese et al. [15] that establishes the effectiveness of GGA functionals. A 90-atom supercell random approximate (SCRAP) is optimized with energy and force convergence criteria of 10^{-8} eV and 10^{-6} eV/Å, respectively [16]. A Monkhorst-Pack *k*-mesh of $6 \times 6 \times 2$ is used for Brillouin-zone integration during structural-optimization and charge self-consistency [17]. Refer supplementary methods for more details.

3. Results and discussion

Fig. 1a shows a relaxed hcp structure of AZ80 alloy, Mg atoms occupy high-symmetry points, with slight displacements in vicinity of Al and Zn on structural relaxation. This observation suggests a change in local Mg-X (X = Al,Zn) bonding. We find significantly reduced bond-length for Mg-X (X = Al,Zn) compared to Mg-Mg (Supplementary

* Corresponding authors at: Ames Laboratory, U.S. Department of Energy, Iowa State University, Ames, IA 50011 USA (P. Sharma).
E-mail addresses: psh@iastate.edu (P. Sharma), psingh84@ameslab.gov (P. Singh).

https://doi.org/10.1016/j.matlet.2024.136501
Received 19 February 2024; Accepted 18 April 2024
Available online 19 April 2024

Table 1), which is attributed to large elemental electronegativity (χ) difference between Mg(1.293) and {Al(1.613), Zn(1.588)} on Allen scale. This large χ variance leads to enhanced charge activity about {Al, Zn} resulting into smaller bond-length, i.e., higher bonding strength.

3.1. Electronic structure analysis

Electronic-structure for metals impacts both physical and chemical properties of an alloy [18]. Therefore, we analyze the electronic band structure and density of states of AZ80. Within the band structure, in Fig. 1b, we find that Mg-s states contribute at lower energies, whereas the Mg-p states contribute to the proximity of the Fermi energy. The projected-DOS for the individual elements (Fig. 1b) reveals that due to the low concentration of Al and Zn, their DOS exhibit diminished electronic states. Since Mg-(s,p) have increased electronic density due to higher concentration as reflected in the projected DOS, Mg has more influence on the electronic structure of AZ80. Nonetheless, the effect of Al or Zn cannot be discounted as they provide stronger hybridization evinced by the overlapping Mg-3(s,p) and Al-3p/Zn-3d states at/near −1.1 and −4.7 eV on the energy scale. This result corroborates that electronic structure effectively directs to the microscopic factors underlying alloy properties.

The absence of translational symmetry is a defining characteristic of random-substitutional alloys, where varying atomic distribution gives rise to a polymorphous configuration that leads to inhomogeneity in the local environment. Hence, we unfold the bands to unravel the intricacies associated with the element specific bands and the role of specific electronic-states towards the properties of AZ80. In Fig. 1c, we map the unfolded supercell band-structure onto a primitive *hcp* Brillouin zone. The bands assuming stronger intensities effectively hybridize especially along M−K in the energy range −2 to 3.3 eV, which is also seen in band-structure. The reconstruction or unfolding of energy-bands [E(*k*)] from DFT calculated bands [E(*K*)] helps to identify the impurity bands of Zn/Al, that is difficult to isolate in the band-structure of a large unit cell.

From the 2D projected charge density plots, Fig. 2a and b, we find that the Mg atoms around Al/Zn show distorted charge with less distortion near Mg-Mg pairs. AZ80 is a dilute alloy so in our 90-atom cell we do not include significant Al-Al and Zn-Zn charges to assess the local atomic charge behavior; however, an analysis of the Mg-X neighborhood suitably establishes the role of electronegativity driven charge-transfer that contributes to solid-solution strengthening. For completeness, in Fig. 2c and d, we present 3D and 2D projected Fermi-surfaces at a constant energy describing the alloy's global characteristics. The presence of electron/hole pockets in Fig. 2d indicates enhanced metallic

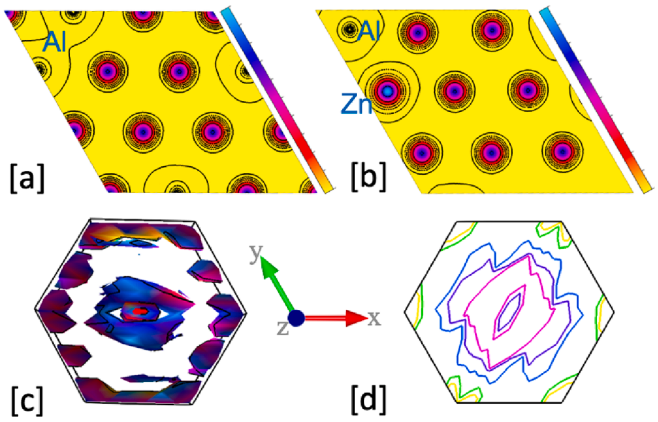

Fig. 2. (a, b) A 2D projected charge-density showing Al-Mg and Zn-Mg planes. (c) 3D and (d) 2D projected fermi-surface of AZ80.

behavior in the x-y plane as reflected from the charge density plots and is expected to govern AZ80 transport properties such as conductivity.

3.2. Phonons (structural) analysis

The phonon spectra are pivotal in disordered alloys influencing structural stability as well as thermal and mechanical behavior. In Fig. 3, we reproduce the phonon dispersion and unfolded phonon bands mapped on the primitive Mg unit cell. The phonons reveal no imaginary (unstable) modes that can give rise to dynamic instability in the crystal lattice, asserting the stability of the *hcp* crystallographic phase. A peak in the phonon DOS for Zn and Al corresponds to a straight band at 1 THz

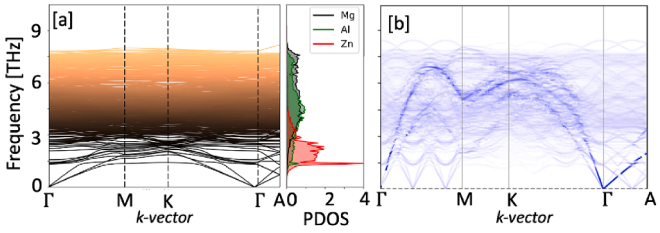

Fig. 3. (a) Phonon dispersion and elemental (Mg, Al, Zn) partial density of states (PDOS), and (b) unfolded phonon dispersion per atom for AZ80.

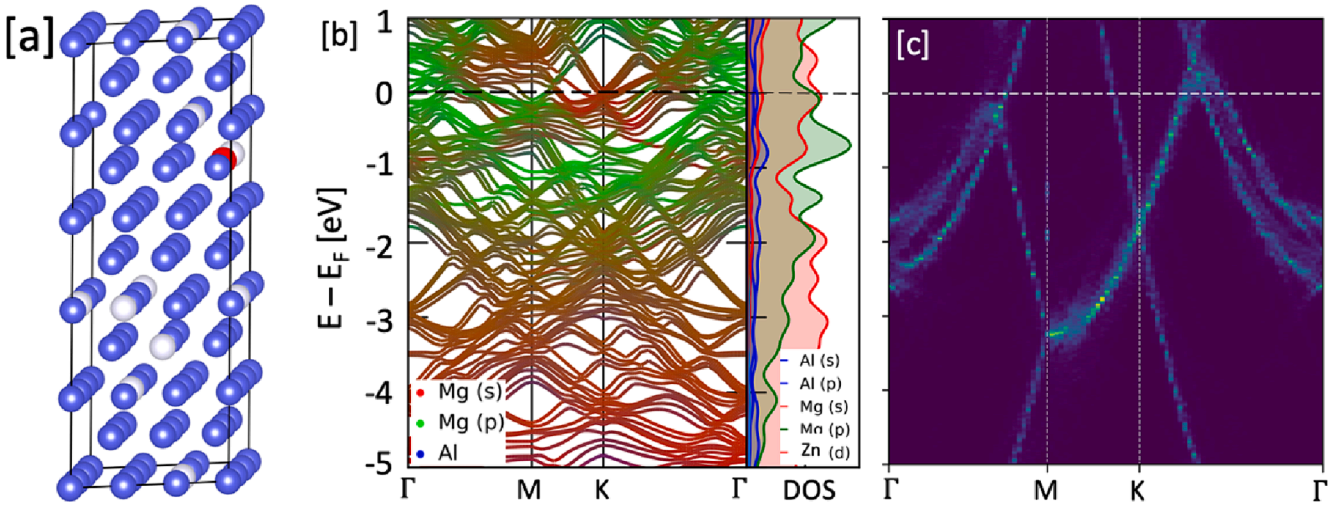

Fig. 1. (a) Relaxed crystal structure of AZ80. The structural parameters area listed in Supplementary Table 1. (b) Electronic structure (bands) and partial density of states (DOS) from −5 to 1 eV for Mg-*(s,p)* and Al-*(s,p)* band crossings at the Fermi energy (E_F). (c) Bands unfolded into the Brillouin zone of primary unit-cell.

between M and K points. Elemental specific phonon density of states in Fig. 3a, indicates that the heavier Zn atoms predominantly contribute to lower frequencies, while lighter Mg and Al atoms contributions are noted at higher frequencies. Zn displays maximum vibrations in the 1 to 3 THz range, while Al and Mg vibrations occur above 3 THz (optical modes). It is worth highlighting the absence of any intersection between the optical and acoustic branches in the phonon dispersion, further substantiating the alloy stability and reporting a clear distinction between the vibrations associated with different elements.

Finally, we assess the mechancial property of AZ80 alloy. The DFT optimzed AZ80 supercell was used to calculate elastic tensors including Young's (DFT=38 GPa; Expt=44.8 GPa) and shear (DFT=14,2 GPa; Expt=17 GPa) modulus for AZ80, see Supplementary Table 2 for more details. The Pugh's ratio, a ductility indicator, was calculated for AZ80 (B/G=2.7) taking the ratio of bulk-moduli (38.3 GPa) vs shear moduli (14.3 GPa), which hints towards ductile nature (B/G $>$ 1.8 is ductile; B/G $<$ 1.8 is brittle). Notably, the 7% tensile elongations reported experimentally [19] agrees with our predictions. The lower shear (14.8 GPa) compared to pure Mg (16.4 GPa) is indicative of the lower barrier for dislocation motion across the *hcp* slip planes under tensile strain, i.e., enhanced ductility over Mg. Note that the limited ductility of pure Mg is attributed to the inability of the *hcp* phase to deform plastically [20].

4. Summary

We present results from a detailed first principles study on the electronic-structure, lattice vibrational spectra (phonons), and mechanical property analysis of light weight Mg-based commercial grade AZ80 alloy. Our results corroborate that dilute alloying by Al/Zn is the key reason that improves the mechanical property such as ductility and strength of AZ80 compared to pure Mg. We attribute this improvement to enhanced charge activity between Al/Zn and Mg due to large electronegativity difference, which agrees with recent reports where ductility is correlated to similar charge-driven mechanisms in metallic alloys [21]. The band unfolding presented for the electrons and phonons is a pivotal step in bridging the gap between theoretical predictions and experimental observations. Our unfolding analysis for AZ80 not only enables a ground for comparison but also contributes significantly to the interpretation of real effects of scattering mechanisms that can help tailor thermo-electro-elastic properties.

CRediT authorship contribution statement

Prince Sharma: Conceptualization, Data curation, Formal analysis, Investigation, Methodology, Validation, Visualization, Writing – original draft, Writing – review & editing. **Duane D. Johnson:** Conceptualization, Formal analysis, Funding acquisition, Project administration, Supervision, Writing – review & editing. **Ganesh Balasubramanian:** Formal analysis, Funding acquisition, Resources, Supervision, Writing – review & editing, Conceptualization. **Prashant Singh:** Conceptualization, Data curation, Formal analysis, Funding acquisition, Investigation, Methodology, Project administration, Resources, Supervision, Validation, Visualization, Writing – original draft, Writing – review & editing.

Declaration of competing interest

The authors declare that they have no known competing financial interests or personal relationships that could have appeared to influence the work reported in this paper.

Data availability

Data will be made available on request.

Acknowledgements

Work at Ames Laboratory was supported by the U.S. Department of Energy (DOE) Office of Science, Basic Energy Sciences, Materials Science & Engineering Division. Part of the research was performed at Iowa State University and Ames Laboratory, which is operated by ISU for the U.S. DOE under contract DE-AC02-07CH11358. PSh and GB acknowledge support from NSF through Grant no. 1944040.

Appendix A. Supplementary data

Supplementary data to this article can be found online at https://doi.org/10.1016/j.matlet.2024.136501.

References

[1] M. Esmaily, J.E. Svensson, S. Fajardo, N. Birbilis, G.S. Frankel, S. Virtanen, R. Arrabal, S. Thomas, L.G. Johansson, Fundamentals and advances in magnesium alloy corrosion, Prog Mater Sci 89 (2017) 92–193, https://doi.org/10.1016/j.pmatsci.2017.04.011.
[2] A.A. Luo, Applications: aerospace, automotive and other structural applications of magnesium, in: Fundamentals of Magnesium Alloy Metallurgy, Elsevier, 2013, pp. 266–316, https://doi.org/10.1533/9780857097293.266.
[3] P. Sharma, N. Naushin, S. Rohila, A. Tiwari, Magnesium Containing High Entropy Alloys, in: Magnesium Alloys Structure and Properties, IntechOpen, 2022. https://doi.org/10.5772/intechopen.98557.
[4] C. Shuai, S. Li, S. Peng, P. Feng, Y. Lai, C. Gao, Biodegradable metallic bone implants, Mater Chem Front 3 (2019) 544–562, https://doi.org/10.1039/C8QM00507A.
[5] B. Akyuz, Influence of Al content on machinability of AZ series Mg alloys, Transactions of Nonferrous Metals Society of China 23 (2013) 2243–2249, https://doi.org/10.1016/S1003-6326(13)62724-7.
[6] Y. Zhou, P. Mao, Z. Wang, L. Zhou, Z. Liu, F. Wang, Solidification process and hot tearing behaviors of AZ series magnesium alloys, Mater Res Express 6 (2019) 116554, https://doi.org/10.1088/2053-1591/ab2bc3.
[7] P. Singh, A.L. Ames, C. Acemi, A. Kuchibhotla, B. Vela, P. Sharma, W. Zhang, P. Mason, G. Balasubramanian, I. Karaman, R. Arroyave, M.C. Hipwell, D.D. Johnson, M. Chandross, Alloying Effects on the Transport Properties of Refractory High-entropy Alloys, (2024). https://doi.org/https://dx.doi.org/10.2139/ssrn.4723754.
[8] G.P. Srivastava, The Physics of Phonons, Routledge (2019), https://doi.org/10.1201/9780203736241.
[9] G. Kresse, J. Furthmüller, Efficient iterative schemes for ab initio total-energy calculations using a plane-wave basis set, Phys Rev B 54 (1996) 11169, https://doi.org/10.1103/PhysRevB.54.11169.
[10] G. Kresse, D. Joubert, From ultrasoft pseudopotentials to the projector augmented-wave method, Phys Rev B 59 (1999) 1758, https://doi.org/10.1103/PhysRevB.59.1758.
[11] J.P. Perdew, K. Burke, M. Ernzerhof, Generalized gradient approximation made simple, Phys Rev Lett 77 (1996) 3865, https://doi.org/10.1103/PhysRevLett.77.3865.
[12] P. Singh, M.K. Harbola, M. Hemanadhan, A. Mookerjee, D.D. Johnson, Better band gaps with asymptotically corrected local exchange potentials, Phys Rev B 93 (2016) 085204, https://doi.org/10.1103/PhysRevB.93.085204.
[13] P. Singh, M.K. Harbola, B. Sanyal, A. Mookerjee, Accurate determination of band gaps within density functional formalism, Phys Rev B 87 (2013) 235110, https://doi.org/10.1103/PhysRevB.87.235110.
[14] P. Söderlind, P.E.A. Turchi, A. Landa, V. Lordi, Ground-state properties of rare-earth metals: an evaluation of density-functional theory, J. Phys. Condensed Matter 26 (2014) 416001, https://doi.org/10.1088/0953-8984/26/41/416001.
[15] T.J. Giese, D.M. York, A GPU-Accelerated Parameter Interpolation Thermodynamic Integration Free Energy Method, J Chem Theory Comput 14 (2018) 1564–1582, https://doi.org/10.1021/acs.jctc.7b01175.
[16] R. Singh, A. Sharma, P. Singh, G. Balasubramanian, D.D. Johnson, Accelerating computational modeling and design of high-entropy alloys, Nat Comput Sci 1 (2021) 54–61, https://doi.org/10.1038/s43588-020-00006-7.
[17] H.J. Monkhorst, J.D. Pack, Special points for Brillouin-zone integrations, Phys Rev B 13 (1976) 5188, https://doi.org/10.1103/PhysRevB.13.5188.
[18] P. Singh, A.V. Smirnov, D.D. Johnson, Ta-Nb-Mo-W refractory high-entropy alloys: Anomalous ordering behavior and its intriguing electronic origin, Phys Rev Mater 2 (2018) 055004, https://doi.org/10.1103/PhysRevMaterials.2.055004.
[19] T.R. Long, C.S. Smith, Single-crystal elastic constants of magnesium and magnesium alloys, Acta Metallurgica 5 (1957) 200–207, https://doi.org/10.1016/0001-6160(57)90166-9.
[20] Z. Wu, W.A. Curtin, The origins of high hardening and low ductility in magnesium, Nature 526 (2015) 62–67, https://doi.org/10.1038/nature15364.
[21] P. Singh, B. Vela, G. Ouyang, N. Argibay, J. Cui, R. Arroyave, D.D. Johnson, A ductility metric for refractory-based multi-principal-element alloys, Acta Mater 257 (2023) 119104, https://doi.org/10.1016/j.actamat.2023.119104.